

中国激光

35 钢/Q355B 钢窄间隙摆动激光填丝焊研究

方荣超¹, 张军², 曾军河³, 宋之克¹, 樊宇^{2*}, 彭文斌³, 安泽²

¹徐州徐工挖掘机械有限公司, 江苏 徐州 221011;

²中国矿业大学材料与物理学院, 江苏 徐州 221116;

³无锡庆源激光科技有限公司, 江苏 无锡 214000

摘要 采用窄间隙摆动激光填丝焊实现了环形工件焊缝成形, 被焊工件为 22 mm 厚 Q355B 钢管与 35 钢环形铸件, 采用 1 道自熔打底焊和 6 道填丝焊完成焊接, 然后通过拉伸、弯曲、冲击性能及显微硬度评定了接头的力学性能。结果表明: 35 钢/Q355B 钢焊接接头表面成形良好, 表面无咬边、焊瘤, 侧壁、层间无气孔及未熔合现象; 35 钢侧热影响区由残余奥氏体、铁素体、少量马氏体和魏氏体组成, Q355B 钢侧热影响区由板条马氏体、少量粒状贝氏体和铁素体组成, 焊缝区主要由珠光体、粒状贝氏体、针状铁素体和回火马氏体组成; 拉伸试样均断裂在母材处, 冲击性能符合相关标准, 试样弯曲后表面未产生明显裂纹, 说明焊接接头的力学性能良好; 通过改变焊接参数可以降低热影响区的硬度。

关键词 激光技术; 窄间隙; 激光填丝焊; 环形焊缝; 力学性能; 显微组织

中图分类号 TG456.7

文献标志码 A

DOI: 10.3788/CJL202249.1602014

1 引言

近年来, 随着激光器应用的普及, 以激光作为热源的焊接方法得到飞速发展。与传统的焊接方法相比, 激光焊接作为一种新的焊接方法, 具有热输入小、焊接效率高、成形质量好等特点^[1-3]。高功率激光器的应用使激光焊接技术得到了进一步发展, 在窄间隙激光填丝焊接过程中, 高功率激光照射焊丝使其熔化并与母材熔合在一起, 克服了工件装配间隙容忍度小、焊接板材较薄等缺点; 同时, 通过填充焊丝可以改变或控制焊缝金属的成分、组织和性能等^[4-6]。

碳钢已被广泛用于制造矿山机械、压力容器、变电站、桥梁等的结构部件。工程机械领域会涉及大量中厚板的焊接, 窄间隙激光填丝焊接技术为中厚板焊接提供了新的解决思路。传统的厚板焊接技术有焊条电弧焊、钨极氩弧焊、埋弧焊等, 窄间隙激光填丝焊接作为一种新兴的厚板焊接方法, 将成为传统焊接技术的可替代选择。

窄间隙激光填丝焊接面临着诸多难题, 热影响区、层间组织淬硬, 侧壁、层间未熔合以及易产生气孔等阻碍着该技术的进一步应用^[7-8]。文献[9]对 16 mm 厚 Q355E 板材的对接焊进行了研究, 结果显示: 焊缝填充区域的组织主要由针状铁素体、粒状贝氏体和珠光体组成, 热影响区组织为回火马氏体及残余奥氏体; 接

头的平均抗拉强度为 521.5 MPa, 接头弯曲后未出现明显开裂, 力学性能良好。文献[10]研究了送丝速度和焊接速度对 Q345E 窄间隙激光填丝焊缝成形的影响。文献[11]基于数值模拟研究了焊接速度对填充激光焊接熔池动态行为的影响。文献[12]对 16 mm 厚 9Ni 钢板材进行焊接后发现, 热影响区主要由马氏体和少量残余奥氏体组成, 焊接接头的硬度值最大可达 340 HV。文献[13-14]分别对 KMn 钢板和锰钢激光自熔焊接头的组织和性能进行研究, 结果表明, 当能量密度较高时, 接头组织中的马氏体尺寸较大, 硬度下降。文献[15-16]研究了激光-电弧复合焊接对异种焊接接头力学性能及组织的影响, 结果表明, 复合焊接接头组织较单纯激光焊接接头组织更粗大, 硬度更高, 且复合焊接接头中出现了 Cr、Ni 元素偏析。文献[17-19]认为采用窄间隙激光填丝焊接方法对碳钢材料进行焊接后, 热影响区的马氏体含量较多, 故其硬度高于母材。

目前, 国内外对窄间隙激光填丝焊接技术所涉及的焊接参数、坡口类型等问题研究得较为深入, 而针对实际工程机械应用类零部件的焊接研究开展得较少。环形工件的窄间隙激光填丝焊接对坡口及加工精度的要求极高, 摆动激光工艺对坡口间隙容忍度高, 而且可以促进侧壁熔合, 较其他焊接方法更具优势。鉴于此, 本团队以工程机械领域常用的 35 钢、Q355B 钢为研

收稿日期: 2021-11-04; **修回日期:** 2021-11-29; **录用日期:** 2021-12-27

基金项目: 国家重点研发计划(2018YFB2001200)、中央高校基本科研业务费学科前沿科学研究专项面上项目(2019XKQYMS10)、江苏省研究生科研与实践创新计划(KYCX21_2201)

通信作者: *fanyu@cumt.edu.cn

研究对象,采用窄间隙摆动激光填丝焊接方法对环形工件进行焊接,探究该技术对环形工件焊接的可行性。

2 研究方法及试验过程

2.1 试验材料

试验材料为 22 mm 厚 Q355B 钢和 35 钢。焊丝牌号为 ER50-6,直径为 1.2 mm。焊丝 ER50-6、Q355B 钢及 35 钢的化学成分如表 1 所示。

表 1 焊丝及母材的化学成分

Table 1 Chemical composition of welding wire and base metal

Element	Mass fraction / %		
	ER50-6 welding wire	Q355B steel	35 steel
C	0.07	0.16	0.36
Mn	1.49	1.45	0.62
Si	0.88	0.16	0.26
S	0.009	0.004	0.003
P	0.012	0.02	0.021
Cr	0.015	0.02	0.08
Ni	0.007	0.01	0.01
Cu	0.12	0.01	0.01
V	0.001	0.01	
Al			0.014
Ti		0.019	
Nb		0.013	
Fe	Balance	Balance	Balance

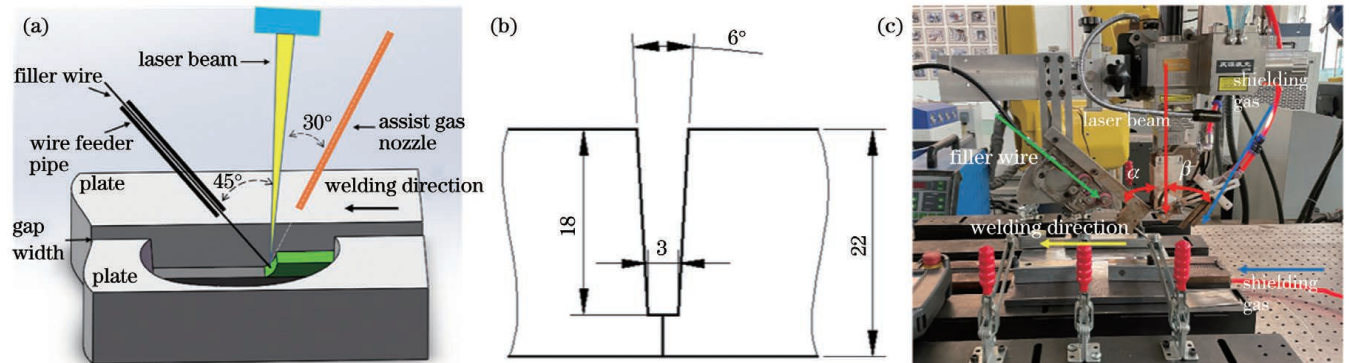


图 1 窄间隙摆动激光焊接。(a)焊接示意图;(b)坡口尺寸;(c)窄间隙摆动激光焊接装置

Fig. 1 Narrow-gap wobble laser welding. (a) Welding diagram; (b) groove geometry; (c) experimental setup of narrow-gap wobble laser welding

表 2 窄间隙摆动激光填丝焊工艺参数

Table 2 Narrow-gap wobble laser filler wire welding process parameters

Pass No.	P /kW	V_w /($m \cdot min^{-1}$)	V_f /($m \cdot min^{-1}$)	f /mm	A /mm	Heat input /($kJ \cdot cm^{-1}$)
1	3.6	0.6		+3	1.0	3.24
2-4	3.6	0.48	4.4	+15	1.5	4.05
5-6	3.8	0.6	4.8	+15	1.5	3.42
7	3.8	0.6	4.6	+25	2.0	3.42

Notes; P represents power; V_w represents welding speed; V_f represents wire feeding rate; f represents defocusing length; A represents amplitude.

2.4 力学性能测试

根据 GB/T 29710—2013《电子束及激光焊接工艺评定试验方法》,采用窄间隙摆动激光填丝焊以对接

2.2 试验设备及方法

试验采用的窄间隙摆动激光填丝焊接试验平台由 YLS-4000-S2T(加装 IPG D30 wobble)、FANUC M-20iA 机器人、WF25i REEL R 送丝机、激光焊接枪体、窄间隙送丝送气系统及焊接工装夹具等搭建而成,其最大输出功率为 4 kW,焦距为 300 mm,未开启振镜且离焦量为 0 时光斑直径为 0.15 mm,保护气体为纯氩气(纯度为 99.999%)。本次试验采用对接形式焊接,焊接示意图如图 1(a)所示。22 mm 厚焊接板材所开坡口形式如图 1(b)所示。本次试验的目的是通过对板材进行对接焊以及对前人研究成果进行研究,探索出 22 mm 厚板材的焊接工艺,并将该工艺应用到环形工件的焊接上。

接头的焊接道数为 7 道。为保证焊缝成形良好,第 1 道采用激光自熔焊,第 2~7 道采用填丝焊,振镜摆动频率为 60 Hz,保护气流量为 15 L/min,其他焊接工艺参数如表 2 所示。

2.3 接头组织观察与分析

在 35 钢/Q355B 钢焊接接头上截取中间部分制备金相试样,采用 4% 硝酸酒精溶液进行腐蚀,然后在 Olympus-GX53 金相显微镜下对接头的微观组织进行观察和分析。

方式进行焊接试验。根据 GB/T 2651—2008《焊接接头拉伸试验方法》制取 4 个拉伸试样,然后采用 YNS 1000 型电液伺服万能试验机进行拉伸试验。根据

GB/T 2653—2008《焊接接头弯曲试验方法》制取 4 个正弯试样,然后采用 YNS 1000 电液伺服万能试验机进行弯曲试验。根据 GB/T 2650—2008《焊接接头冲击试

验方法》制取 6 个冲击试样,缺口位于焊缝中心,然后采用 Jb-500b 摆锤式冲击试验机进行室温冲击试验,试验温度为 23 ℃。力学性能试样示意图如图 2 所示。

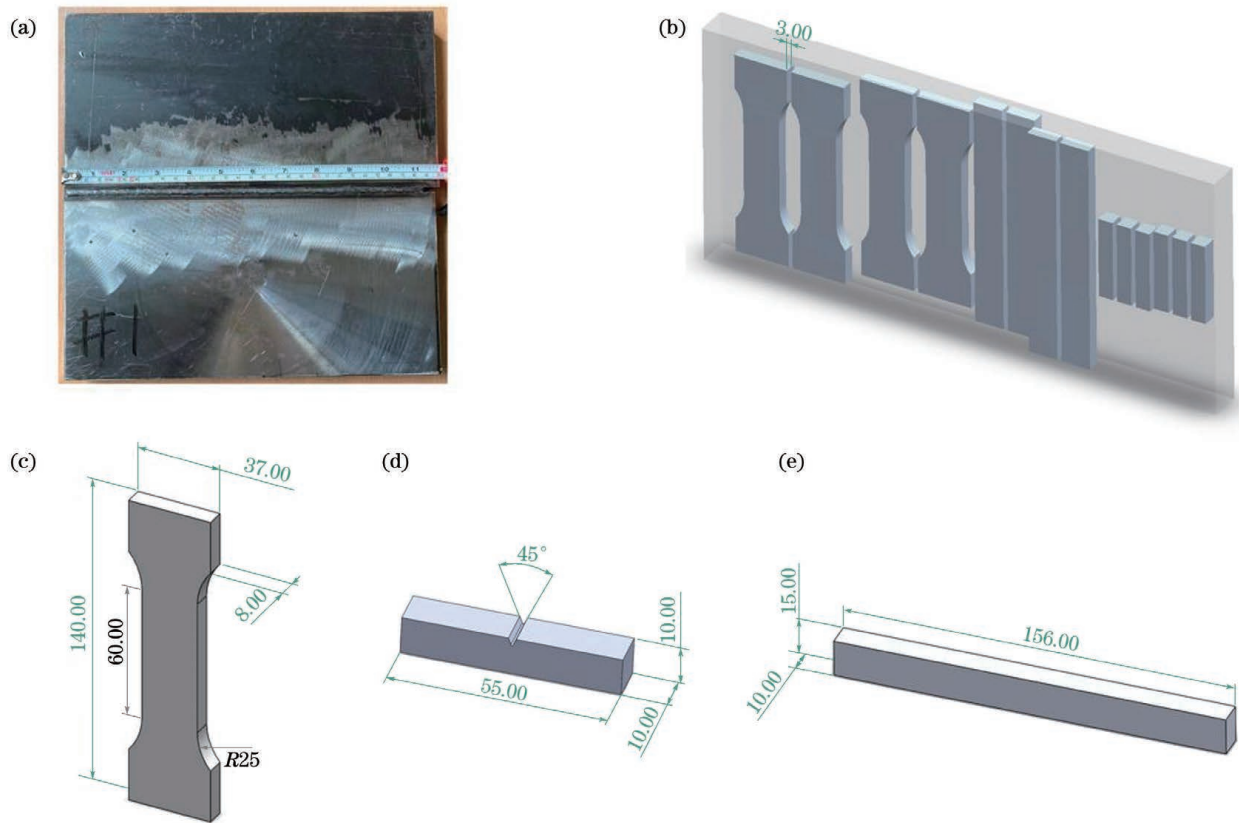


图 2 力学性能试样示意图。(a)焊接试板;(b)取样示意图;(c)拉伸试样示意图;(d)弯曲试样示意图;(e)冲击试样示意图
Fig. 2 Schematics of samples for mechanical properties testing. (a) Welding test plate; (b) sampling diagram; (c) schematic of tensile sample; (d) schematic of bending sample; (e) schematic of impact sample

3 实验结果及分析

35 钢、Q355B 钢的显微组织如图 3 所示。35 钢、Q355B 钢均由铁素体与珠光体组成。试验用 35 钢经

过了锻后调质处理,珠光体呈大块片状,铁素体呈网状且不规则地分布于珠光体晶界处,为易淬火钢。试验用 Q355B 钢经过了轧制,珠光体与铁素体呈带状分布,为不易淬火钢。

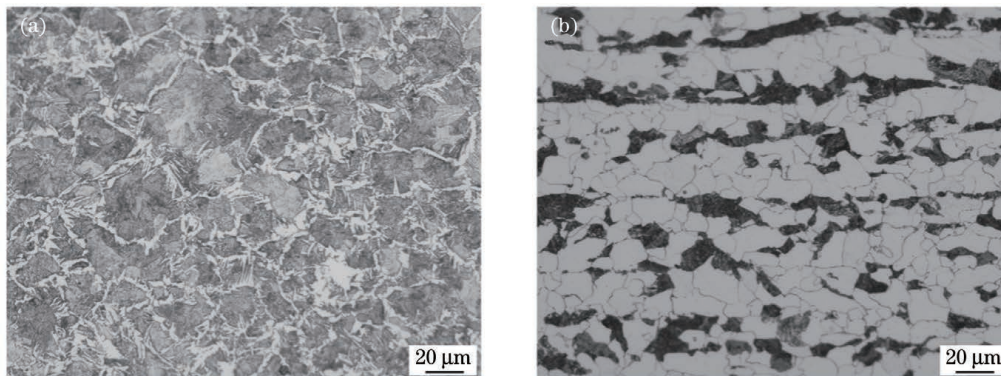


图 3 母材的显微组织。(a)35 钢;(b)Q355B 钢

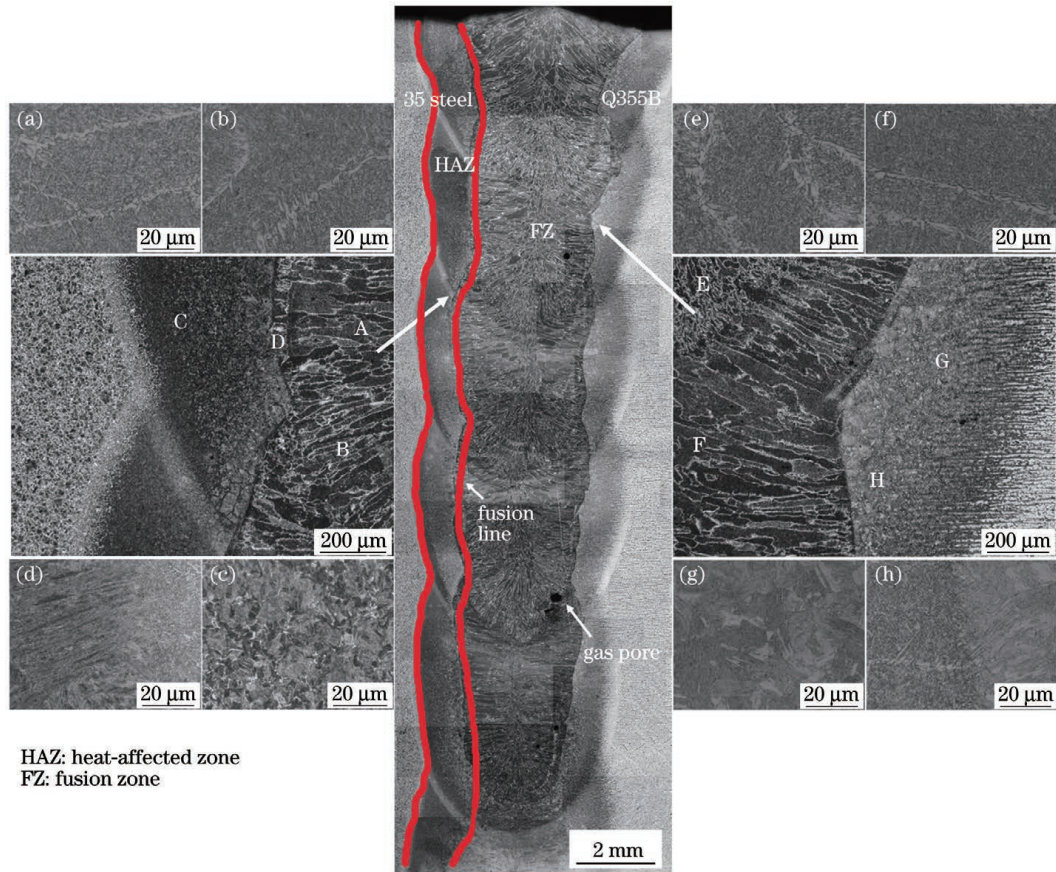
Fig. 3 Microstructures of base materials. (a) 35 steel; (b) Q355B steel

3.1 宏观形貌与微观组织分析

35 钢/Q355B 钢窄间隙摆动激光填丝焊接接头的宏观形貌如图 2(a)所示,通过探伤检测可知焊缝内部无贯穿性气孔裂纹,侧壁无未熔合等缺陷,焊缝表面光滑平整。这表明采用合适的窄间隙摆动激光填丝焊接

工艺参数和焊接流程可以保证平板接头的焊接质量。

焊接接头的微观组织如图 4 所示,焊缝左侧为 35 钢,右侧为 Q355B 钢。焊接接头侧壁熔合较好,Q355B 钢侧的热影响区宽度较 35 钢侧大,热影响区最大宽度为 1.1 mm,最大熔深为 4.87 mm。激光填



HAZ: heat-affected zone
FZ: fusion zone

图 4 35 钢/Q355B 钢异种接头横截面的显微组织, (a)~(h) 分别为 A~H 区的放大图

Fig. 4 Cross-section microstructure of 35 steel/Q355B steel dissimilar joint, where images (a)~(h) are enlarged views of zones A-H

丝焊接过程中的冷速很快, 熔池中产生的气体无法充分逸出, 因此, 焊缝中部形成了少量尺寸较小的非贯穿性气孔。35 钢侧 A 区为焊丝填充区, 该区域主要由大量细小的针状铁素体以及先共析铁素体、回火马氏体组成; B 区为层间区域, 前层焊道顶端部分熔化, 冷却后熔合线不清晰, 熔合线外侧的较窄区域受后一道焊接附加的热处理作用, 相当于进行了一

次正火处理, 细化了晶粒, 受热程度低于上层焊丝填充区, 且冷速较缓, 可观察到该区域的铁素体晶粒较细小; C 区域为不完全淬火区, 主要由残余奥氏体、铁素体及少量马氏体组成, 电镜下的显微组织如图 5(b) 所示; D 区域为完全淬火区, 晶粒较为粗大, 由魏氏体、针状铁素体及马氏体组成, 电镜下的显微组织如图 5(a) 所示。

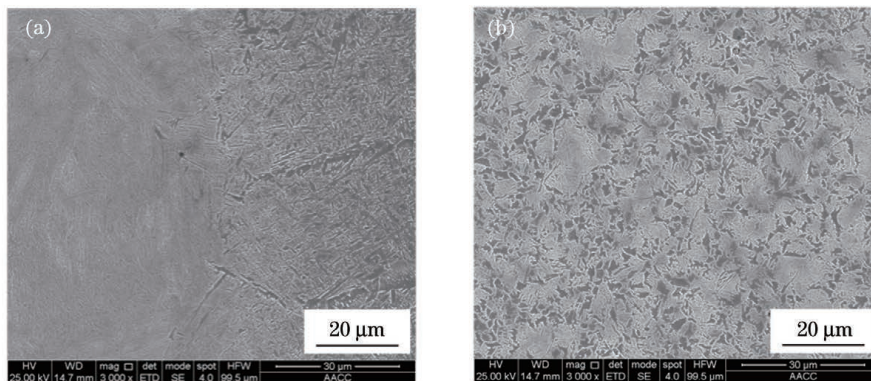


图 5 焊接接头 35 钢侧热影响区的显微组织。(a) 熔合线处的显微组织; (b) 热影响区中部的显微组织

Fig. 5 Microstructures of heat-affected zone on 35 steel side of welded joint. (a) Microstructure of fusion line; (b) microstructure of the middle of heat-affected zone

Q355B 钢侧 E、F 区的组织分布及形貌同 35 钢侧 A、B 区的相同; G 区为不完全重结晶区, 晶粒大小不规则, 该部分奥氏体的均匀化程度较低, 部分晶粒长大

严重, 铁素体呈不规则带状分布于晶界处, 珠光体与母材相比发生粗化, 电镜下的显微组织如图 6(b) 所示; H 区为过热区, 由板条状马氏体、少量粒状贝氏体及

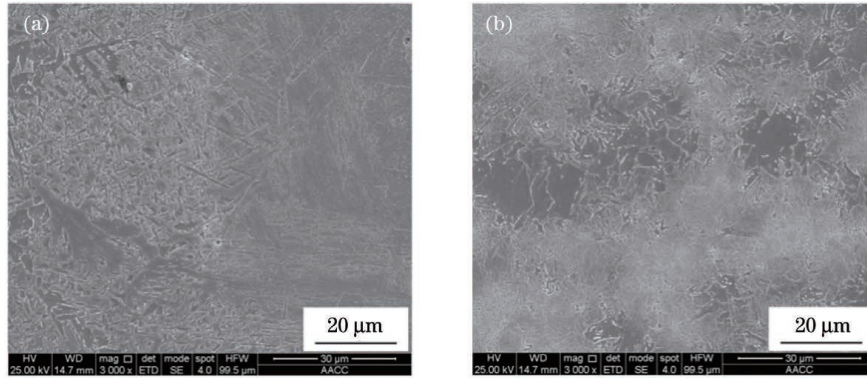


图 6 焊接接头 Q355B 钢侧热影响区的显微组织。(a)熔合线处的显微组织;(b)热影响区中部的显微组织
Fig. 6 Microstructures of heat-affected zone on Q355B steel side of welded joint. (a) Microstructure of fusion line; (b) microstructure of the middle of heat-affected zone

铁素体组成(粒状贝氏体及铁素体具有较好的韧性,可以降低熔合线处的裂纹扩展倾向),电镜下的显微组织如图 6(a)所示。

3.2 力学性能分析

拉伸试验结果如表 3 所示,焊接接头的抗拉强度均值为 553.5 MPa,焊接接头拉伸试样均断裂在母材处,Q355B 母材断裂的倾向更大,焊接接头的抗拉强度均优于 Q355B、35 钢母材。

表 3 拉伸试验结果

Table 3 Tensile testing results

No.	Yield strength	Tensile strength	Fracture location	Elongation δ / %
	R_e /MPa	R_m /MPa		
1	384	550	Q355B steel	20.3
2	419	549	35 steel	21.8
3	398	552	Q355B steel	20.3
4	457	563	Q355B steel	19.5

焊接接头的弯曲试验结果如图 7 所示,弯曲试样侧弯 90°后均未开裂。

焊接接头冲击试样在 23 °C 下的冲击吸收功在

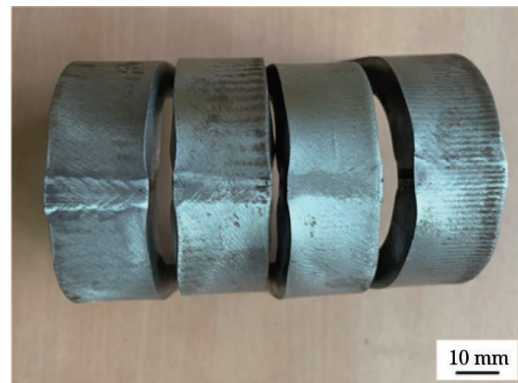


图 7 弯曲试样图

Fig. 7 Bending sample diagram

94.6~121.3 J 之间。图 8 为冲击断口区的电镜形貌。焊缝上部的断口上分布着尺寸较深的韧窝,该部分区域的组织为大量针状体铁素体及分布均匀的粒状贝氏体,这种组织特征增加了焊接接头处的韧性;此外,该部分断口上出现撕裂形貌,说明这部分区域的冲击韧性较好。焊缝底部自熔焊区的断口较平滑,这部分区域的组织主要由马氏体构成,脆性较大,如图 8(b)所示,断口表面无明显的撕裂形貌,说明其冲击韧性较差。

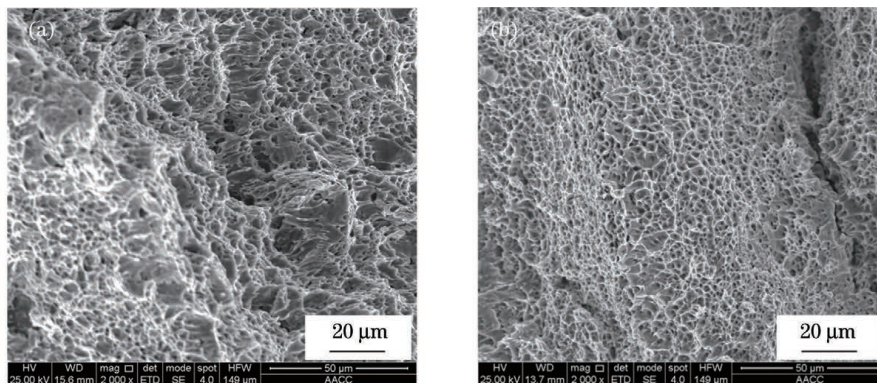


图 8 冲击断口的电镜形貌。(a)焊缝上部;(b)焊缝底部

Fig. 8 Scanning electron microscopy (SEM) images of impact fracture. (a) Upper layer of welded joint; (b) bottom layer of welded joint

焊接接头的硬度分布如图 9 所示。可见:焊接接头上、中、底部硬度差值较明显,底部自熔焊区的硬度

明显高于填丝焊接区。自熔焊接的冷速较填丝焊接大得多,冷却过程中主要生成板条状马氏体,且马氏体含

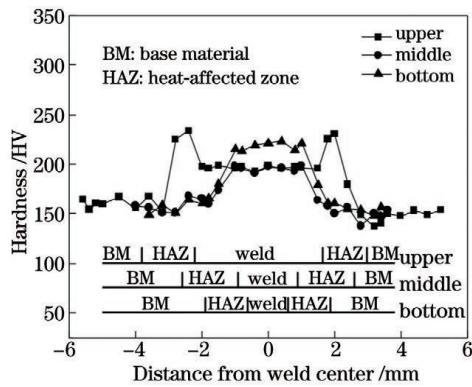


图 9 焊接接头的硬度分布

Fig. 9 Hardness distribution of welded joint

量较高,同时自熔焊接的焊缝宽度较窄,因此底部焊缝区的硬度较高。填丝部位热影响区的硬度明显高于母

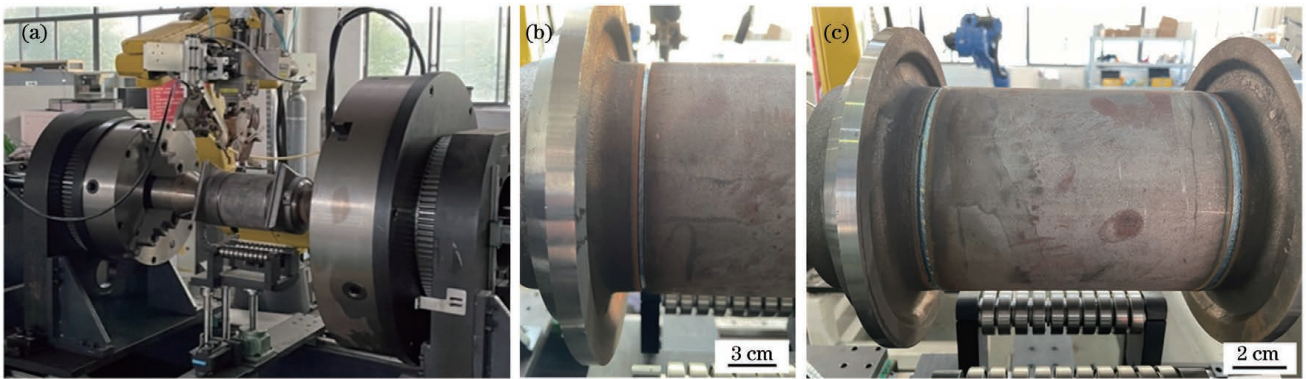


图 10 环形工件的焊接。(a)窄间隙摆动激光填丝焊接实验设备;(b)焊缝底部;(c)焊缝表面

Fig. 10 Welding of circular workpiece. (a) Experimental setup for narrow-gap wobble laser welding; (b) bottom layer of welded joint; (c) surface layer of welded joint

4 结 论

本团队使用摆动激光填丝焊接方法实现了 35 钢/Q355B 钢异种接头的对接焊,分析了接头的力学性能和显微组织,得出以下结论:

1) 通过优化工艺参数,采用摆动激光填丝焊接对 35 钢和 Q355B 钢管进行焊接,总计焊接 7 道次,焊接接头力学性能良好,抗拉、弯曲、硬度性能均符合相关标准。

2) 摆动激光填丝焊接工艺可使熔池在焊接过程中被充分搅拌,促进了气孔逸出和侧壁熔合;通过降低线性热输入,热影响区的马氏体得以细化,针状铁素体及粒状贝氏体含量增加;中间层热影响区经过了二次热循环,粗大晶粒得以细化,硬度降低明显。

3) 窄间隙摆动激光焊接可以有效克服坡口容忍度小、加工过程不稳定等缺点,可得到侧壁、层间熔合良好的焊接接头,适合环形工件的焊接。

参 考 文 献

- [1] Zhao Y, Ma S C, Huang J, et al. Narrow-gap laser welding using filler wire of thick steel plates [J]. The International Journal of Advanced Manufacturing Technology, 2017, 93(5/6/7/8): 2955-2962.
- [2] Zhang C, Li G, Gao M, et al. Microstructure and mechanical properties of narrow gap laser-arc hybrid welded 40 mm thick mild steel [J]. Materials, 2017, 10(2): 106.
- [3] Yang W X, Xin J J, Fang C, et al. Microstructure and mechanical properties of ultra-narrow gap laser weld joint of 100 mm-thick SUS304 steel plates [J]. Journal of Materials Processing Technology, 2019, 265: 130-137.
- [4] 徐望辉, 杨清福, 肖逸峰. 窄间隙焊接侧壁熔合控制技术研究现状 [J]. 精密成形工程, 2020, 12(4): 47-54.
Xu W H, Yang Q F, Xiao Y F. Research status of sidewall fusion control technology in narrow gap welding [J]. Journal of Netshape Forming Engineering, 2020, 12(4): 47-54.
- [5] 孙旭, 张林杰, Suck-Joo Na. 功率密度对 DP590 钢激光焊缝熔深及组织的影响 [J]. 精密成形工程, 2020, 12(1): 111-116.
Sun X, Zhang L J, Suck-Joo N. Effect of power density on penetration depth and microstructure in laser welding joint of DP590 steel [J]. Journal of Netshape Forming Engineering, 2020, 12(1): 111-116.
- [6] 耿志杰, 王善林, 陈玉华, 等. 不同填充材料下 316LN/Inconel 718 异种激光焊接头的显微组织与力学性能 [J]. 精密成形工程, 2019, 11(5): 71-77.
Geng Z J, Wang S L, Chen Y H, et al. Microstructure and mechanical properties of 316LN/Inconel 718 dissimilar alloy laser welding joint with different filling materials [J]. Journal of Netshape Forming Engineering, 2019, 11(5): 71-77.
- [7] 张成竹, 陈辉. B950CF 高强度超窄间隙激光焊接头组织对残余应力的影响 [J]. 中国激光, 2021, 48(6): 0602101.
Zhang C Z, Chen H. Effect of microstructures of ultranarrow

- gap laser welded B950CF steel joints on residual stress distribution [J]. Chinese Journal of Lasers, 2021, 48(6): 0602101.
- [8] 孙清洁, 李军兆, 刘一搏, 等. 电磁场辅助 SUS316L 不锈钢扫描激光窄间隙焊接接头成形及组织性能 [J]. 中国激光, 2020, 47(10): 1002005.
Sun Q J, Li J Z, Liu Y B, et al. Formation, microstructure, and properties of electromagnetic field-assisted SUS316L austenite stainless steel laser narrow-gap joint [J]. Chinese Journal of Lasers, 2020, 47(10): 1002005.
- [9] 阚晓阳, 汪认, 叶结和, 等. 转向架用 Q345E 钢窄间隙激光填丝焊接接头组织和力学性能研究 [J]. 热加工工艺, 2018, 47(7): 244-246, 251.
Kan X Y, Wang R, Ye J H, et al. Microstructure and mechanical properties of narrow-gap laser welding joint with filler wire of Q345E steel for bogies [J]. Hot Working Technology, 2018, 47(7): 244-246, 251.
- [10] 李德利. 送丝及焊接速度对 Q345E 窄间隙激光填丝焊缝成形的影响 [J]. 电焊机, 2018, 48(7): 80-84.
Li D L. Effect of wire feed speed and welding speed on Q345E narrow gap laser filler wire weld formation [J]. Electric Welding Machine, 2018, 48(7): 80-84.
- [11] 彭进, 许红巧, 王星星, 等. 焊接速度对填材填充激光焊接熔池动态行为影响的数值模拟 [J]. 中国激光, 2020, 47(3): 0302005.
Peng J, Xu H Q, Wang X X, et al. Numerical simulation of influence of welding speed on dynamic behavior of laser welding molten pool with filler metal [J]. Chinese Journal of Lasers, 2020, 47(3): 0302005.
- [12] 田书强, 李铸国, 华学明. 9Ni 钢超窄间隙光纤激光焊接接头组织及性能 [J]. 激光与光电子学进展, 2017, 54(4): 041408.
Tian S Q, Li Z G, Hua X M. Microstructure and property of 9Ni steel joint by ultra-narrow-gap fiber laser welding [J]. Laser & Optoelectronics Progress, 2017, 54(4): 041408.
- [13] 邓德伟, 吕捷, 马玉山, 等. 激光焊接 KMN 钢的工艺参数及组织和性能 [J]. 焊接, 2020(5): 10-16, 61.
Deng D W, Lü J, Ma Y S, et al. Process parameters, microstructures and mechanical properties of KMN steel by laser welding [J]. Welding & Joining, 2020(5): 10-16, 61.
- [14] 曹洋, 赵琳, 彭云, 等. 热输入对激光焊中锰钢接头组织和力学性能的影响 [J]. 中国激光, 2018, 45(11): 1102008.
Cao Y, Zhao L, Peng Y, et al. Effect of heat input on microstructure and mechanical properties of laser welded medium Mn steel joints [J]. Chinese Journal of Lasers, 2018, 45(11): 1102008.
- [15] Zhang X, Mi G Y, Wang C M. Microstructure and performance of hybrid laser-arc welded high-strength low alloy steel and austenitic stainless steel dissimilar joint [J]. Optics & Laser Technology, 2020, 122: 105878.
- [16] 严春妍, 易思, 张浩, 等. S355 钢激光-MIG 复合焊接头显微组织和残余应力 [J]. 焊接学报, 2020, 41(6): 12-18, 97.
Yan C Y, Yi S, Zhang H, et al. Investigation of microstructure and stress in laser-MIG hybrid welded S355 steel plates [J]. Transactions of the China Welding Institution, 2020, 41(6): 12-18, 97.
- [17] 汪认, 阚晓阳, 叶结和, 等. SMA490BW 耐候钢窄间隙激光填丝焊接接头组织与性能 [J]. 焊接技术, 2017, 46(10): 25-28.
Wang R, Kan X Y, Ye J H, et al. Microstructure and properties of narrow gap laser wire filled welding joints of SMA490BW weathering steel [J]. Welding Technology, 2017, 46(10): 25-28.
- [18] 李涛, 朱忠尹, 邢艳双, 等. S355J2N 钢窄间隙激光填丝焊接头力学性能及微观组织研究 [J]. 电焊机, 2018, 48(12): 98-103.
Li T, Zhu Z Y, Xing Y S, et al. Research on mechanical properties and microstructure of the ultra-narrow gap laser wire filler welding joint for the S355J2N steel [J]. Electric Welding Machine, 2018, 48(12): 98-103.
- [19] 邓平, 皇甫乐森, 马生翀, 等. 20 钢管-Q345C 钢管窄间隙激光焊接接头组织与性能 [J]. 焊接技术, 2019, 48(2): 8-10, 44.
Deng P, Huangfu Y S, Ma S C, et al. Microstructure and properties of narrow gap laser welded joints of 20 steel-Q345C tube [J]. Welding Technology, 2019, 48(2): 8-10, 44.

Narrow Gap Wobble Laser with Filling Wire for Welding of 35 Steel and Q355B Steel

Fang Rongchao¹, Zhang Jun², Zeng Junhe³, Song Zhike¹, Fan Yu^{2*}, Peng Wenbin³, An Ze²

¹ Xuzhou XCMG Excavator Machinery Company Limited, Xuzhou 221011, Jiangsu, China;

² School of Materials and Physics, China University of Mining and Technology, Xuzhou 221116, Jiangsu, China;

³ Wuxi Qingyuan Laser Technology Company Limited, Wuxi 214000, Jiangsu, China

Abstract

Objective The welding technology that uses lasers as a heat source has advanced quickly in recent years as laser applications have become more popular. Laser welding has various advantages over traditional welding techniques, including minimal heat input, high efficiency, and good quality. Narrow gap laser (NGL) with filler wire will replace existing traditional welding methods as a new thick plate welding method. However, many challenges [hardening of the heat-affected zone (HAZ) and interlayer structure, lack of fusing of the sidewall and interlayer, porosity, and so on] hinder its further development. This study investigated the welding of shaft parts for real construction machinery to address the problem of high groove and machining accuracy requirements in NGL. The wobbling laser process was used to improve the groove gap tolerance and promote sidewall fusion. This study examined and discussed the dissimilar joint between Q355B steel and 35 steel tubes welded using NGL.

Methods To weld the dissimilar joint of Q355B steel and 35 steel tubes with 22 mm thickness, 1 pass self-melting and 6 passes filling wire were used. According to relevant national standards, the tensile test, bending test, impact test, and microhardness measurement were conducted to evaluate the mechanical properties of joints. The cross-sections of the

welded joints were ground, polished, and etched with 4% nitric acid alcohol solution. Weld seams microstructures were examined using an Olympus-GX53 optical microscope and a Quanta 250 field emission scanning electron microscope. The Wilson VH1102 semi-automatic tester was used to measure the microhardness distributions at the welded joints with a load of 0.5 N and a dwell time of 10 s. The YNS 1000 universal testing machine was used to perform tensile and bending tests. The impact test was performed using a Jb-500b pendulum impact testing machine.

Results and Discussions There are no defects, such as penetration pores and cracks, lack of fusion for sidewall, and so on, inside the samples after non-destructive testing. The width of HAZ near Q355B has a wider breadth than that of the HAZ near 35 steel. Zone A is the fusing zone of the filling wire around 35 steel, as shown in Fig. 4. This region is mainly made up of a large number of fine acicular ferrite, proeutectoid ferrite, and tempered martensite. The interlayer area is designated as zone B. The top section of the previous weld bead is remelted, and the interlayer fusion line is not visible after cooling. The narrow area outside the fusion line is subjected to the additional heat treatment by next pass welding, which is equivalent to a normalizing treatment and results in grain refinement. Zone B has a lower heating degree than the upper welding wire-filled area, and the cooling rate is slow (Fig. 4).

The properties of tensile, impact, and bending specimens have superior qualities to those of basic metal. The microhardness difference of welded joint section is larger, and the hardness of the rear welding zone is greater than that of the weld zone.

The actual shaft parts were welded relying on the accumulation of previous experiments. The NGL with wire filling welding method was used to weld the shaft components without pausing by matching the welding parameters with the chuck speed (Fig. 10).

Conclusions In this study, through the use of ER50-6 welding wire for NGL with filler wire butt welding of 35 steel and Q355B steel, the mechanical properties and microstructure can be analyzed, and the following conclusions can be drawn: (1) By optimizing the process parameters, the 35 steel and Q355B steel pipes were welded using the wobbling laser filler wire welding method, a total of 7 welding passes, the mechanical properties of the welded joints are great, and the tensile, bending and hardness properties are all up to the relevant national standards; (2) The wobble laser welding process is adopted to fully stir the molten pool throughout the welding process to promote and increase pore escape and sidewall fusion. Reduced linear heat input refines the heat-affected zone martensite and increases the content of acicular ferrite and granular bainite. The heat-affected zone structure in the middle layer undergoes a second thermal cycle, the coarse grains are refined, and the hardness is significantly reduced; (3) The narrow gap wobbling laser welding method successfully overcomes the shortcomings such as small groove tolerance and unstable processing, resulting in excellent sidewall and interlayer fusion of the welded joint, and a laser welding process for the narrow gap on the shaft components is proposed.

Key words laser technique; narrow gap; laser welding with filling wire; circular weld; mechanical properties; microstructure